Monolayer calibration of endofullerenes with x-ray absorption from implanted keV ion doses

Wei Chuang Lee,[1] Lebin Yu,[1] Johan Oscarsson,[2] Michal W. Ochapski,[3] Ryunosuke Sagehashi,[1] Yang Zhang,[4] Alexey A. Popov,[4] Zewdu M. Gebeyehu,[3] Leonardo Martini,[3] Stiven Forti,[3] Camilla Coletti,[3] Bernard Delley,[5] Matthias Muntwiler,[5] Daniel Primetzhofer,[2] and Thomas Greber[1]

[1)] *Physik-Institut, University of Zürich, CH-8057 Zürich, Switzerland*
[2)] *Department of Physics and Astronomy, Uppsala University, 75120, Sweden*
[3)] *Graphene Labs, Istituto Italiano di Tecnologia, Genova, Italy*
[4)] *Leibniz-Institute for Solid State and Materials Research (IFW), D-01069 Dresden, Germany*
[5)] *Swiss Light Source, Paul Scherrer Institut (PSI), CH-5232 Villigen, Switzerland*

(*Electronic mail: weichuang.lee@physik.uzh.ch)

(Dated: 22 December 2023)

X-ray absorption spectroscopy (XAS) has the highest sensitivity for chemical element detection on surfaces. With this approach, small amounts of the lanthanide-containing endofullerene molecules ($Ho_3N@C_{80}$) have been measured by total electron yield at a low flux bending magnet beamline. The monolayer coverage is calibrated by extrapolating the signals of constant doses (3×10^{14} cm^{-2}) of Ho ions implanted into SiO_2 with energies between 2 and 115 keV. At room temperature, the Ho XAS spectra of the molecules and implanted ions indicate trivalent but not identical Ho ground states. Still, this approach demonstrates a way for calibration of small coverages of molecules containing open core-shell elements.

Most studies of molecules on surfaces require the determination of the molecular coverage. There are various techniques to determine the thickness or number of layers of the surface, including x-ray photoemission spectroscopy (XPS)[1], scanning tunneling microscopy (STM)[2], atomic force microscopy (AFM)[3], low energy electron diffraction (LEED)[4] and x-ray diffraction[5].

X-ray absorption spectroscopy (XAS) across resonance has the highest elemental sensitivity among the coverage determination methods as can be seen in the tabulated x-ray attenuation coefficients[6]. At resonance, i.e. for direct transitions between occupied and unoccupied atomic orbitals the absorption is particularly high. This involves a tuneable x-ray source that allows for a resonant excitation process with a high cross section[7] but more signal as compared to non-resonantly excited photo-electrons in XPS. As it is known for XPS, XAS accesses the electronic structure and chemical bonding of molecules[8] as well and is particularly useful for the study of systems close to the detection limit. This limit is not only given by the number of atoms to be probed, but also limited by the background of the other atoms that are hit by the x-rays. For the present problem of monolayer or sub-monolayer investigation, it is best for x-ray absorption to make use of concomitant electron yield detection, since the electrons in the relevant energy range have a mean free path closer to the layer thickness than x-ray photons. The highest surface sensitivity would be obtained by the direct measurement of the Auger electrons that relax the given x-ray excitation[9], while the detection of the total electron yield (TEY) is also more surface sensitive than the measurement of the x-ray fluorescence, which is best suited for systems with thicknesses corresponding to the x-ray attenuation length.

The superior sensitivity of XAS applies to the present case of monolayers and submonolayers of endofullerene molecules with lanthanides as endohedral units, for example, $DySc_2N@C_{80}$ that has been investigated for the single-molecule magnet behavior[10].

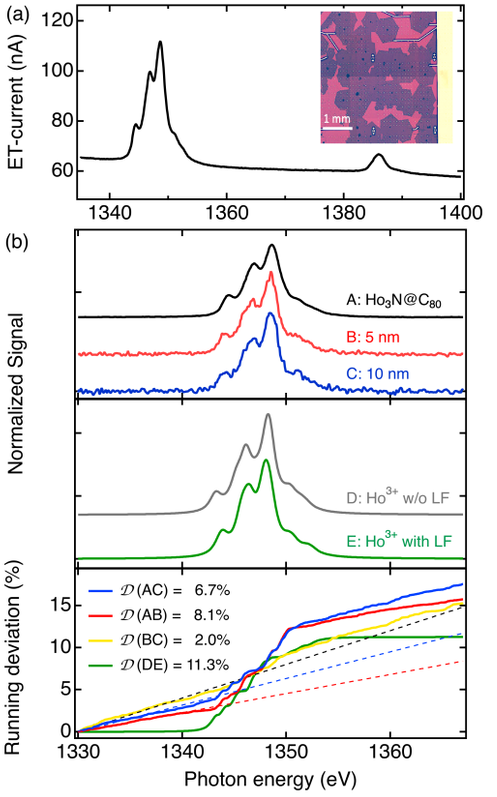

FIG. 1. *(a) Sum of 30 XAS scans of the Ho $M_{4,5}$ edge with 1000 data points at room temperature of $Ho_3N@C_{80}$ recorded as total current by the Everhard-Thornley (ET) detector. Inset: Optical microscope image of graphene and gold contacts on a SiO_2/Si sample. The dark hexagonal regions represent single-crystalline monolayer graphene, the lighter regions are the bare SiO_2, and the bright bar on the right is the gold contact. (b) Top panel: Ho M_5 XAS data (spec A) from (a); 5nm (spec B), and 10nm (spec C) implanted layers with offsets. Middle panel: Calculated Ho XAS multiplet spectra of Ho^{3+} without (spec D) and Ho^{3+} with ligand field (LF) (spec E). Bottom panel: Running deviations as described in Ref [11]. The corresponding statistical noise is indicated by dashed lines. Blue: Deviation $\mathscr{D}$ between spectrum A and C, Red: A and B, Yellow: B and C, Green: D and E, are listed in %.*

For the case of $Ho_3N@C_{80}$ the Ho $M_{4,5}$ edge has a high cross-section, and it is furthermore known that the sensitivity of XAS to the light polarization may give information on the lanthanide ligand field and the 4f orbital orientation with respect to the light polarization vector[12,11,13].

We have demonstrated before that high-quality XAS signals at a low flux bending magnet beamline can be obtained by implementing an Everhard-Thornley (ET) detector for the total electron yield[14]. Measuring the thickness of a multilayer compound with XPS can be involved although the photoemission cross sections and electron mean free paths are well known[15]. The short electron mean free path provides high surface sensitivity, though different models, such as layer by layer or cluster growth, provide different results. On the other hand, the longer probing depth of XAS that is performed with TEY is less sensitive to influence of the details of the growth model on the layer thickness and provides robust surface density numbers of elements, if the signal may be calibrated. As we show here, the monolayer $Ho_3N@C_{80}$ XAS signal may be accurately calibrated from the extrapolation of the Ho signal of defined Ho ion doses that have been implanted with different energies. We measured XAS of the Ho M_5 and, for comparison, the Si K-edge of the SiO_2/Si substrate as a function of Ho implantation depth. This enabled us to determine the coverage of the evaporated molecule sample on gMOS devices and as an intermediate of the determination of the probing depth of TEY on SiO_2.

The study is carried out at the Photoemission and Atomic Resolution Laboratory (PEARL) beamline at the Swiss light source[16], with photon energies from 1330 eV to 1860 eV, with a beam spot size of about 200 µm × 100 µm on the sample at the normal incidence. $Ho_3N@C_{80}$ molecules first dissolved in toluene are loaded in a Knudsen cell and evaporated in-situ on the target at 750 K for 10 mins, about 15 mm away[17].

The inset in Figure 1(a) shows the microscope image of the target which consists of single-layer graphene (dark region) with Au-contacts on graphene/SiO_2 to ground the graphene. The tiny darker spots in the center of the individual hexagons are considered to be bilayer graphene[18]. Figure 1(a) depicts the Ho $M_{4,5}$ edge XAS spectrum that is a sum of 30 scans measured by the Everhard-Thornley detector[19]. One way to eliminate the background noise from the XAS spectrum is by fitting and dividing it with a 5-order polynomial function while excluding the Ho $M_{4,5}$ edge[14]. After background removal and normalization, Figure 1(b) displays the M_5 edge spectrum from Figure 1(a) as a black curve and two spectra of implanted Ho with energies of 2 and 8 keV, where the Ho^{3+} ions are implanted into SiO_2 5 nm and 10 nm below the surface, respectively, which the Ho ions were implanted using a high-current 350 kV Danfysik implanter at the tandem laboratory of Uppsala University[20]. Implantations were performed in 2 mm × 2 mm patches masked by an aluminium foil employing a scanned beam.

The running deviation shows the integral of the absolute value of the difference between two spectra after background removal and normalization[11]. In Figure 1(b), discernible differences between the two spectra become evident within the Ho M_5 edge region.

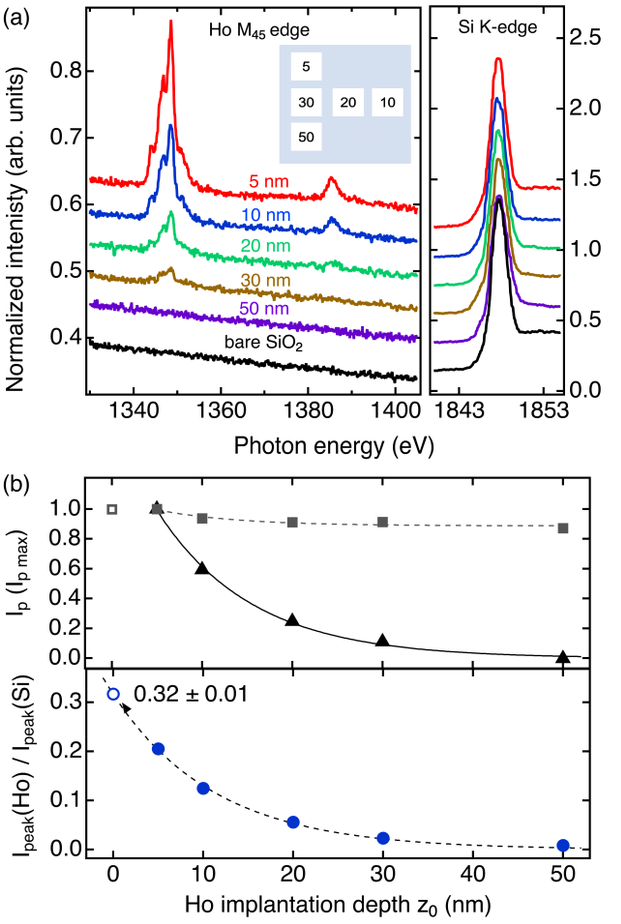

FIG. 2. *(a) Left panel: XAS spectra of Ho $M_{4,5}$ edge for different implantation depth of Ho on a SiO_2 substrate, with a dose of 3×10^{14} cm^{-2} ions, equivalent to 3 Ho atoms in an ML of C_{80} (⌀ ≈ 1.1nm). Each spectrum is the sum of two XAS scans. The Ho XAS signal is significantly suppressed as the Ho ions are implanted deeper, with almost no Ho M_5 peak observed a depth of 50 nm. Inset: Configuration of the 2mm × 2mm Ho implantation patches on a 10 mm × 10 mm SiO_2 sample. Right panel: XAS of the corresponding Si K-edges. In both panels the individual spectra are offset from the spectra of the bare surface for better visibility. (b) Top panel: Si K-edge peak (square) and Ho M_5 peak (triangle) intensities versus Ho implantation depth z_0. The intensities are normalized with the peak intensity at 5 nm. The dashed lines are the fits between the filled symbols with attenuation depths for secondary electrons $\Lambda_{Si} = 9 \pm 3$ nm, whereas $\Lambda_{Ho} = 10.3 \pm 0.7$ nm. Bottom panel: Peak ratios between the M_5 edge and Si K-edge (filled circle). The dashed line is the exponential fit between 5 and 50 nm that extrapolates to $z_0 = 0$ (empty circle), where the peak ratio is 0.32 ± 0.01.*

The statistical noise is inferred from the data outside of the M_5 edge region $E \notin [1340, 1355]$ eV. The dashed lines are fitted to the segments preceding the Ho M_5 edge $E < 1340$ eV, and those behind the Ho M_5 edge $E > 1355$ eV. The deviation $\mathscr{D}$ in the Ho signal is then determined from the difference between the two lines at the center of the M_5 multiplet.

While the deviation between the 5 nm and 10 nm implantation depths spectra $\mathscr{D}$(BC) in Figure 1(b) has a value of $2.0 \pm 0.1\%$, the deviation between the implanted Ho (spec B)

TABLE I. *Implantation parameters for 3×10^{14} cm^{-2} Ho ions in SiO_2 and observed Ho M_5 and Si K_1 XAS peak intensities. The first row reports the Si K_1 intensity for the bare SiO_2. The STB ratios are the Signal-To-Background ratios at the given peak energies.*

Energy (keV)	Depth (nm)	I_{Si} (peak)	Si STB ratio	I_{Ho} (peak)	Ho STB ratio
-	Surface*	1.190	9.481	-	-
2	5	1.175	8.408	0.252	0.34
8	10	1.095	8.607	0.149	0.18
28	20	1.066	8.104	0.062	0.06
54	30	1.059	8.416	0.028	0.03
115	50	1.019	7.831	0.000	0.00

and the Ho^{3+} ions in the molecule (spec A) amounts to $\mathscr{D}$(AB)= 8.1 $\pm$ 0.1%. While this analysis suggests no difference between spectra of different implantation depth, the difference of the Ho spectrum of the molecules and the implants is small, though significant.

To understand this disparity the multiX software for the calculation of XAS multiplet spectra[21] is used. With this we may infer the same valency of Ho^{3+} valency but a different ligand field. As the ligand field of the Ho in the SiO_2 matrix is expected to be weaker, we calculated Ho^{3+} M_5 multiplets with and without the ligand field known for the molecules at room temperature[13]. The resultant theoretical XAS spectra are displayed in the middle panel of Figure 1(b), and the running deviation may be used to support the hypothesis of a weaker ligand field for Ho in SiO_2 compared to Ho in $Ho_3N@C_{80}$. The deviation amounts to $\mathscr{D}$(DE)=11.3%, close to $\mathscr{D}$(AB)=8.1%. The agreement between the experiments and the proposed model is good and it shows that the running deviation is a sensitive mean to quantify small spectral differences. The higher deviation of the theoretical spectra can be partly attributed to the absence of noise. We like to emphasize that this does not affect the calibration procedure as long as the x-ray absorption cross sections of the two Ho species are the same.

In Figure 2(a), the spectra of the Ho $M_{4,5}$ edge between 5 and 50 nm implantation depth from corresponding implantation energies[22] are presented in the left panel. They indicate a significant decrease in Ho $M_{4,5}$ peak intensity with deeper implantation depths. The right panel of Figure 2(a) displays the Si K-edge XAS spectra taken after the corresponding Ho $M_{4,5}$ edge measurement, showing a less pronounced decrease in Si K_1 peak intensity compared to Ho. The normalized intensities are the ratios between the Everhart-Thornley currents and the mirror currents and for the corresponding peak intensities are summarized in Table 1 together with the signal-to-background ratios and the implantation energies of the ions. The Ho ion energy for a given implantation depth in SiO_2 was determined with the software SRIM (Stopping and Range of Ions in Matter)[23] and is in good agreement with existing Yb implantation data which has been also calculated with Monte Carlo data analysis (TRIM)[22].

In Figure 2(b), we show the decrease in both, the Ho M_5 peak (triangle symbol) and Si K_1 peak (square symbols) normalized intensities with increasing Ho implantation depth. The Si K_1 peak intensity decrease can not be explained by an attenuation of the x-ray beam due to the presence of the Ho, but we propose it to be due to the change of the silicon density[24] in the SiO_2 layer down to the respective implantation depth. Considering this effect, it is possible to fit both, the Ho and Si, peak intensities using the model:

$$I_{Ho} = I_0^{Ho} \cdot exp\Big(-\frac{z_0}{\Lambda_{Ho}}\Big) \quad (1)$$

where I_0^{Ho} is the Ho intensity for implantation depth z_0=0, and Λ_{Ho} is the effective attenuation length (TEY probing depth) of Ho. This is the standard equation for signal attenuation of a δ-layer at z_0[25].
For Si, we do not expect an attenuation if the x-ray attenuation of Ho can be neglected. However, the data indicate a decrease depending on z_0. With this we get:

$$I_{Si} = I_0^{Si} \cdot \Big[\alpha \cdot \Big(1 - exp\Big(-\frac{z_0}{\Lambda_{Si}}\Big)\Big) + exp\Big(-\frac{z_0}{\Lambda_{Si}}\Big)\Big], \quad (2)$$

where I_0^{Si} is the Si intensity for implantation depth z_0=0, and Λ_{Si} the effective attenuation lengths of the Si electron yield. α is the Si density parameter describing the effect of ion penetration down to z_0. The data in Figure 2(b) are fitted with exponential functions as given in Eq. 1 and 2 and yield for the electron cascade attenuation lengths or TEY probing depth Λ_{Ho} = 10.3 $\pm$ 0.7 nm and Λ_{Si} = 9 $\pm$ 3 nm for Ho and Si, respectively. The present TEY probing depth have the same order of magnitude as predicted by the old empirical formula of Reimer cited in[25], i.e. 6 and 8 nm. This emphasizes that the Λ values should be measured, rather than estimated if an accurate coverage calibration shall be performed. The Si K_1 peak intensity (Eq. 2) has a density change parameter α of 0.83 $\pm$ 0.03 which translates to 17% of Si density decrease due to the implantation process. The peak ratio between Ho M_5 and Si K_1 extrapolated to $z_0 = 0$ is the parameter for the determination of the monolayer coverage of the Ho-containing molecules. To this extent, the peak ratio (R) of Ho and Si is shown in the bottom panel of Figure 2(b) with filled circles. The empty circle represents the extrapolated value R(z_0=0)=R_0 after fitting an exponential function, which gives a dimensionless value of R_0=0.32 $\pm$ 0.01. R_0 is determined for every beamline and monochromator setting as long as the photon flux measurement, which was performed in the present case by mirror current measurements, is accurate.

Using the extrapolated R_0 = 0.32 value between the Ho M_5 and the Si K_1 peak, we calibrated the coverage of the $Ho_3N@C_{80}$ molecules evaporated onto the graphene surface in Figure 1(a), where we find $R_0(Ho_3N@C_{80}) = 0.290\pm0.002$. This corresponds to a coverage of 0.91$\pm$0.04 monolayers of $Ho_3N@C_{80}$ molecules. We note that we neglected in this analysis the graphene layer and the rest of the molecules due to the large Λ values.

To summarize, we have demonstrated a non-destructive method to determine the monolayer coverage of small amounts of evaporated lanthanide-containing endofullerene molecules using x-ray absorption spectroscopy (XAS). Through our experiment, we have provided an example of how $Ho_3N@C_{80}$ monolayer coverage calibration can be achieved by measuring peak ratios of Ho M_5 and Si K_1. This

peak ratios are an important piece of information that can facilitate accurate calibration of the coverage, which can also be applied to any small coverage of molecules containing an open core-shell element. Overall, our study highlights the potential of XAS as a reliable and effective technique for measuring the coverage of molecules.

ACKNOWLEDGMENTS

Financial support by the Swiss National Science Foundation grant No. 200020_153312 and No. 200020_201086 are gratefully acknowledged. The Paul Scherrer Institut, Villigen, Switzerland provided synchrotron radiation beamtime at the PEARL beamline. Support of the ion implanter operation at Uppsala University by the Swedish Research Council (VR-RFI contract No. 2019_0019) is also gratefully acknowledged. This research has received funding from the European Union's Horizon 2023 research and innovation program under grant agreement no. 881603-GrapheneCore3.

CONFLICT OF INTEREST

The authors have no conflicts to disclose.

DATA AVAILABILITY

The data that support the findings of this study are available from the corresponding author upon reasonable request.

REFERENCES

[1]D. Y. Zemlyanov, M. Jespersen, D. N. Zakharov, J. Hu, R. Paul, A. Kumar, S. Pacley, N. Glavin, D. Saenz, K. C. Smith, T. S. Fisher, and A. A. Voevodin, "Versatile technique for assessing thickness of 2D layered materials by XPS," Nanotechnology **29**, 115705 (2018).

[2]K. A. Fisher, S. L. Whitfield, R. Thomson, K. C. Yanagimoto, M. G. Gustafsson, and J. Clarke, "Measuring changes in membrane thickness by scanning tunneling microscopy," Biochimica et Biophysica Acta (BBA) - Biomembranes **1023**, 325–334 (1990).

[3]T. H. Kim, H. I. Kwon, J. D. Lee, and B.-G. Park, "Thickness measurements of ultra-thin films using AFM," Digest of Papers. Microprocesses and Nanotechnology , 240–241 (2001).

[4]G. Lee, D. Poker, D. Zehner, and E. Plummer, "Coverage and structure of deuterium on Cu(111)," Surface Science **357-358**, 717–720 (1996).

[5]M. Witte, "Measurement of coating thickness with x-ray diffraction," Powder Diffraction **38**, 112–118 (2023).

[6]J. H. Hubbell and S. M. Seltzer, "X-ray mass attenuation coefficients,".

[7]N. Mårtensson, J. Söderstrom, S. Svensson, O. Travnikova, M. Patanen, C. Miron, L. J. Sæthre, K. J. Børve, T. D. Thomas, J. J. Kas, F. D. Vila, and J. J. Rehr, "On the relation between x-ray photoelectron spectroscopy and XAFS," *Journal of Physics: Conference Series*, **430**, 012131 (2013).

[8]B. T. Thole, G. van der Laan, J. C. Fuggle, G. A. Sawatzky, R. C. Karnatak, and J.-M. Esteva, "3d x-ray absorption lines and the $3d^9 4f^{n+1}$ multiplets of the lanthanides," Phys. Rev. B **32**, 5107–5118 (1985).

[9]M. Treier, P. Ruffieux, R. Fasel, F. Nolting, S. Yang, L. Dunsch, and T. Greber, "Looking inside an endohedral fullerene: Inter- and intramolecular ordering of $dy_3N@c_{80}$ (I_h) on cu(111)," Phys. Rev. B **80**, 081403 (2009).

[10]R. Nakanishi, J. Satoh, K. Katoh, H. Zhang, B. K. Breedlove, M. Nishijima, Y. Nakanishi, H. Omachi, H. Shinohara, and M. Yamashita, "$DySc_2N@C_{80}$ single-molecule magnetic metallofullerene encapsulated in a single-walled carbon nanotube," Journal of the American Chemical Society **140**, 10955–10959 (2018), pMID: 30125097, https://doi.org/10.1021/jacs.8b06983.

[11]T. Greber, A. P. Seitsonen, A. Hemmi, J. Dreiser, R. Stania, F. Matsui, M. Muntwiler, A. A. Popov, and R. Westerström, "Circular dichroism and angular deviation in x-ray absorption spectra of $Dy_2ScN@C_{80}$ single-molecule magnets on $h-BN/Rh(111)$," Phys. Rev. Mater. **3**, 014409 (2019).

[12]R. Westerström, A.-C. Uldry, R. Stania, J. Dreiser, C. Piamonteze, M. Muntwiler, F. Matsui, S. Rusponi, H. Brune, S. Yang, A. Popov, B. Büchner, B. Delley, and T. Greber, "Surface aligned magnetic moments and hysteresis of an endohedral single-molecule magnet on a metal," Phys. Rev. Lett. **114**, 087201 (2015).

[13]R. Sagehashi, W. C. Lee, F. Liu, A. A. Popov, M. Muntwiler, B. Delley, P. Krüger, and T. Greber, "Inferring the Dy-N axis orientation in adsorbed $DySc_2N@C_{80}$ endofullerenes by linearly polarized x-ray absorption spectroscopy," Phys. Rev. Mater. **7**, 086001 (2023).

[14]W. C. Lee, R. Sagehashi, Y. Zhang, A. A. Popov, M. Muntwiler, and T. Greber, "X-ray absorption measurements at a bending magnet beamline with an Everhart–Thornley detector: A monolayer of $Ho_3N@C_{80}$ on graphene," Journal of Vacuum Science Technology A **40**, 053205 (2022).

[15]M. Taskin, Z. Novotny, M. Hengsberger, and J. Osterwalder, "Formation of $Ni_xFe_{3-x}O_4$ (100)," Phys. Rev. Mater. **7**, 055801 (2023).

[16]M. Muntwiler, J. Zhang, R. Stania, F. Matsui, P. Oberta, U. Flechsig, L. Patthey, C. Quitmann, T. Glatzel, R. Widmer, E. Meyer, T. A. Jung, P. Aebi, R. Fasel, and T. Greber, "Surface science at the PEARL beamline of the Swiss Light Source," J. Synchrotron Rad. **24**, 354–366 (2017).

[17]R. Stania, A. P. Seitsonen, H. Y. Jung, D. Kunhardt, B. Buchner, A. A. Popov, M. Muntwiler, and T. Greber, "Temperature induced change of conformation of $Sc_2TbN@C_{80}$ on h-BN/Ni(111)," (2022), 10.48550/ARXIV.2205.07342.

[18]S. Pezzini, V. Mišeikis, G. Piccinini, S. Forti, S. Pace, R. Engelke, F. Rossella, K. Watanabe, T. Taniguchi, P. Kim, and C. Coletti, "30°-twisted bilayer graphene quasicrystals from chemical vapor deposition," Nano Letters **20**, 3313–3319 (2020).

[19]T. E. Everhart and R. F. M. Thornley, "Wide-band detector for micro-microampere low-energy electron currents," Journal of Scientific Instruments **37**, 246–248 (1960).

[20]P. Strom. and D. Primetzhofer, "Ion beam tools for nondestructive in-situ and in-operando composition analysis and modification of materials at the Tandem Laboratory in Uppsala," Journal of Instrumentation **17**, P04011 (2022).

[21]A. Uldry, F. Vernay, and B. Delley, "Systematic computation of crystal-field multiplets for x-ray core spectroscopies," Phys. Rev. B **85**, 125133 (2012).

[22]P. Grande, P. Fichtner, M. Behar, and F. Zawislak, "Range profiles of medium and heavy ions implanted into SiO_2," Nuclear Instruments and Methods in Physics Research Section B: Beam Interactions with Materials and Atoms **35**, 17–20 (1988).

[23]M. Z. J. F. Ziegler, J.P. Biersack, *The stopping and Range of Ions in Matter (SRIM)*.

[24]J. Klappe, I. Bársony, J. Liefting, and T. Ryan, "Optimization of ion implantation damage annealing by means of high-resolution x-ray diffraction," Thin Solid Films **235**, 189–197 (1993).

[25]A. Erbil, G. S. Cargill III, R. Frahm, and R. F. Boehme, "Total-electron-yield current measurements for near-surface extended x-ray-absorption fine structure," Phys. Rev. B **37**, 2450–2464 (1988).